TENSION, COMPRESSION AND SHEAR FATIGUE OF A CLOSED CELL FOAM

Dan Zenkert* and Magnus Burman*
*Kungliga Tekniska Högskolan (KTH), Department of Aeronautical and Vehicle Engineering, SE – 100 44 Stockholm, Sweden

Keywords: *Cellular materials, foam, fatigue, crack propagation*

Abstract

A closed cell foam of Polymetacrylimide (Rohacell) with three different densities is studied. The foam is tested quasistatically in tension, compression and shear. The tensile properties scale very well with the relative density of the foam, but the compression and shear properties do not. It is believed to be due to cell edge and cell wall buckling being the dominated deformation mechanism in compression and shear for lower densities that does not occur for higher densities. Fatigue testing is then performed in tension, compression and shear. It is seen that for all load cases and densities, the fatigue life can be plotted using Basquin's law. The results also show that the different failure mechanisms found in the static tests are the same in fatigue. This means that the fatigue life for different load types exhibit different failure mechanisms. This shows not only as a clear difference in the stress levels for fatigue failure, but also on the slope in the fatigue life relation.

1 Introduction

Rigid cellular foams are extensively used as a structural core in load carrying sandwich structures. The usage stretches over applications in aerospace, automotive, marine, transportation and infra-structure. There are numerous examples of applications and a few worth noticing here are example the new Swedish Navy Corvette Visby, wind-mill blades, and novel train car structures. In all of these and most other foam core sandwich applications, the core is typically a closed cell polymer foam, designed to carry a substantial part of the load. More and more has been focused on the core material recently due to increased demands for material properties and models to use in the design of sandwich structures. Fracture and fatigue of load carrying foam cores remains to a large extent unknown. The reason for this is the inherent structure of foams, constituted of a complicated 3-dimensional network of thin membranes (cell walls), enclosing each cell. At the intersection of cell walls, edges with concentrated mass build up rods or beams. A foam is not just a material, but also a micro-structure – homogeneous continuum or heterogeneous cell structure, depending on the scale of interest.

Not much has been reported on fatigue of foams. Some early work was performed by Burman et al [1-2], Shenoi et al [3]], Buene et al [4] and Kanny and Mahfuz [5]. Kanny and Mahfuz [6] and Kulkarni et al [7] performed fatigue testing of foam core sandwich beams with polymer foam cores. The testing set-up was in all these cases such that the core would be subjected mainly to shear stress and the intention was to find the stress-life curve for shear stress. McCullough et al [8] tested aluminium foams in both tension-tension and compression-compression fatigue. Although the results therein are not given in terms of a Basquins' law it was found that the slope of the S-N curve is considerably lower in the compression-compression fatigue case. Harte et al [9] performed fatigue testing of an open and a closed cell aluminium foam with one aim of finding the fatigue limit. Olurin et al [10] performed crack propagation measurement on two closed cell aluminium foams. Shipsha et al [11,12] used both compact tension (CT) and cracked sandwich beams specimens to measure crack propagation rates in polymer foams. In both cases it was found that the crack rates were considerably higher than for homogeneous solid materials.

By using micro-mechanics Huang and Lin [13] performed the first attempt to model crack propagation in foams and were able to density normalise the data into one single generic relation for all density phenolic foams. Zenkert et al [14] used an initial flaw approach model through which

the crack propagation data could be transformed to stress-life curves. The model gave excellent agreement with measured crack propagation data and tension-tension fatigue testing results for two closed cell polymer foams. In this study we extend the work in [14] to study also fatigue under compressive and shear loading

2 Materials

The high performance closed cell rigid polymer foam Rohacell WF-grade was used. A micrograph of the cell structure of this foam is shown in Fig.1. Rohacell is a Polymetacrylimide (PMI) foam with predominantly closed cells, which is a rather brittle foam with a tensile strain to failure of approximately 2-3%. Details on this material can be found in [15]. Three different densities were used; WF51, WF110 and WF200, with nominal densities of 52, 110 and 205 kg/m^3, respectively.
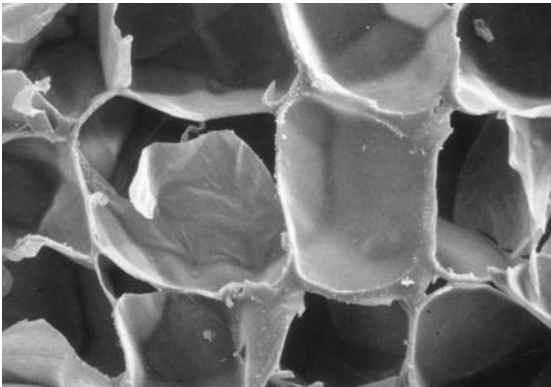
Fig. 1. Cell structure of WF51. (Reprinted with permission of Röhm GmbH)

3 Static Properties

Static properties of the foams used herein were tested in tension, compression and shear. The tension and compression tests were performed using the same specimen geometry as used in the fatigue testing (described below) at a prescribed displacement rate of 1 mm/minute. The static shear properties were obtained from the same four-point bending test as later used in the fatigue testing. In this test one can get the shear strength but not the complete stress-strain relation. However, by reducing the load-displacement relation from the test to shear stress (transverse load per unit width divided by core thickness) and readjusting the displacement values so that the initial slope equals the known shear modulus we can get the complete

curve, at least approximately. Shear tests performed by the core material manufacturer using the standard block shear test according to ASTM-C273 were used for comparison. The reason for using the bend test primarily is that block shear test, because of its design, often gives a non-conservative value, at least in strain to failure, and for high density foams. The stress-strain relations are shown in Fig.2.
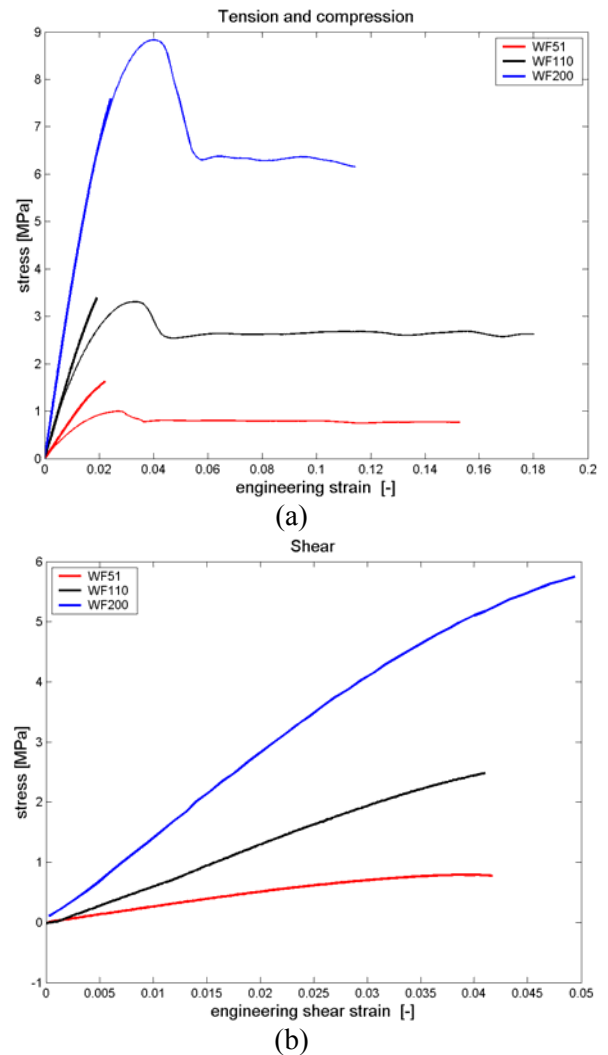

(a)

(b)

Fig. 2. Typical stress-strain relations for WF51, WF110 and WF200 in (a) tension/compression and (b) tension/shear. Tension curves are in thick lines and compression in thin lines

In tension, the material yields, though very little. We have chosen to use the yield stress as the governing parameter rather than the stress at rupture. The yield point in tension has been defined as a standard 0.2% offset stress, a value being very close to the ultimate strength. In subsequent use of this property we will refer to this as the yield strength in tension. The values of yield strength are also given

in Table 1. There are many interpretations of the compressive strength of foams. As seen from Fig. 2, the compressive stress-strain relation can be defined by a linear part, followed by a slight non-linear part, a distinct peak followed by a small stress drop and then a so called plateau level. The manufacturers almost always supply this peak stress in the stress-strain relation as the compressive strength. The material also yields in compression and shear. We have chosen the yield points in compression as a 1% offset stress and in shear as the 0.5% offset stress. There is no particular rationale behind this choice except that these points provide good cut-off stress limits for the fatigue results described in the following sections.

Table 1. Material data for WF51, WF110 and WF200 (manufacturer's data within parenthesis)

	WF51	WF110	WF200
ρ [kg/m^3]	52 (52)	114 (110)	207 (205)
E [MPa]	75 (75)	185 (180)	395 (350)
G [MPa]	27 (24)	71 (70)	152 (150)
$\hat{\sigma}_{tension}$ [MPa]	1.6 (1.6)	3.5 (3.7)	7.4 (6.8)
$\hat{\sigma}_{yield}^{tension}$ [MPa]	1.51	3.20	6.45
$\hat{\sigma}_{compression}$ [MPa]	0.95 (0.8)	3.4 (3.6)	8.9 (9.0)
$\hat{\sigma}_{yield}^{compression}$ [MPa]	0.90	3.2	8.0
$\hat{\tau}_{shear}$ [MPa]	0.75 (0.8)	2.5 (2.4)	6.0 (5.0)
$\hat{\tau}_{yield}^{shear}$ [MPa]	0.66	2.4	5.8
$\hat{\sigma}_{compression} / \hat{\sigma}_{tension}$	0.50	0.97	1.32
$\hat{\tau}_{shear} / \hat{\sigma}_{tension}$	0.50	0.73	0.77
$E / \overline{\rho}^n$	2370	2550	2760
$G / \overline{\rho}^n$	760	990	1050
$\hat{\sigma}_{tension} / \overline{\rho}^n$	50	51	48
$\hat{\sigma}_{compression} / \overline{\rho}^n$	25	50	63
$\hat{\tau}_{shear} / \overline{\rho}^n$	25	33	35

In [14] the tensile stress-strain relations were normalised with the density and shown to form a generic relation. The density normalisation was performed using

$$\overline{x} = \alpha\overline{\rho}^n \qquad (1)$$

where $\overline{x}$ is some mechanical property of the foam normalised with its value for the fully dense material (bulk property) of which the cell edges and faces are made of, and $\overline{\rho}$ is the foam density normalised with the bulk density of the material, the latter taken as 1200 kg/m^3. This scaling works well when having $n = 1.1$ for properties like elastic modulus and tensile strength. The actual numbers are included in Table 1. In [14] it was shown that other properties, like fracture toughness, also scale similarly well.

Typical stress-strain relations are given in Fig. 2. For reasons of discussion these are plotted in two graphs. In Fig. 2a the tensile and compression relations are shown together and in Fig. 2b the shear relations are shown. By density normalizing according to eq.(1), the tensile stress-strain relations will almost perfectly overlap for all three densities, as seen in Fig.3a. One can also see from Table 1 that both the elastic modulus and the tensile strength have almost the same normalised number for all three densities. However, the shear strength and compressive strength do not appear to scale the same way. This is seen in Figs.3b and c. The lowest density, WF51, has considerably lower strength and stiffness in shear and compression as compared to its tensile values (see Table 1). For WF200 the situation is almost the opposite, at least the compressive strength is higher than its tensile strength. The reason for this is not proven, but can be explained by the following; the cell wall material is the same for all densities. Higher densities have smaller cells and thicker cell edges and cell walls. Following the procedures by Gibson and Ashby [16] it can be identified that for an idealised open cell foam the cell edge buckling stress is proportional to the relative density square ($\overline{\rho}^2$). A similar reasoning for an idealised closed cell foam would give that cell wall buckling is proportional to the relative density cube ($\overline{\rho}^3$). Thus, buckling is most likely the dominating triggering mechanism for failure in compression for the low density foam, but not for higher densities. Shear loading, being a combination of tension and compression, should then exhibit the same principal mechanism. There are some hints to this in the stress-strain relations given in Fig. 2 as well.

Rohacell normalised tensile data

(a)

Rohacell normalised compression data

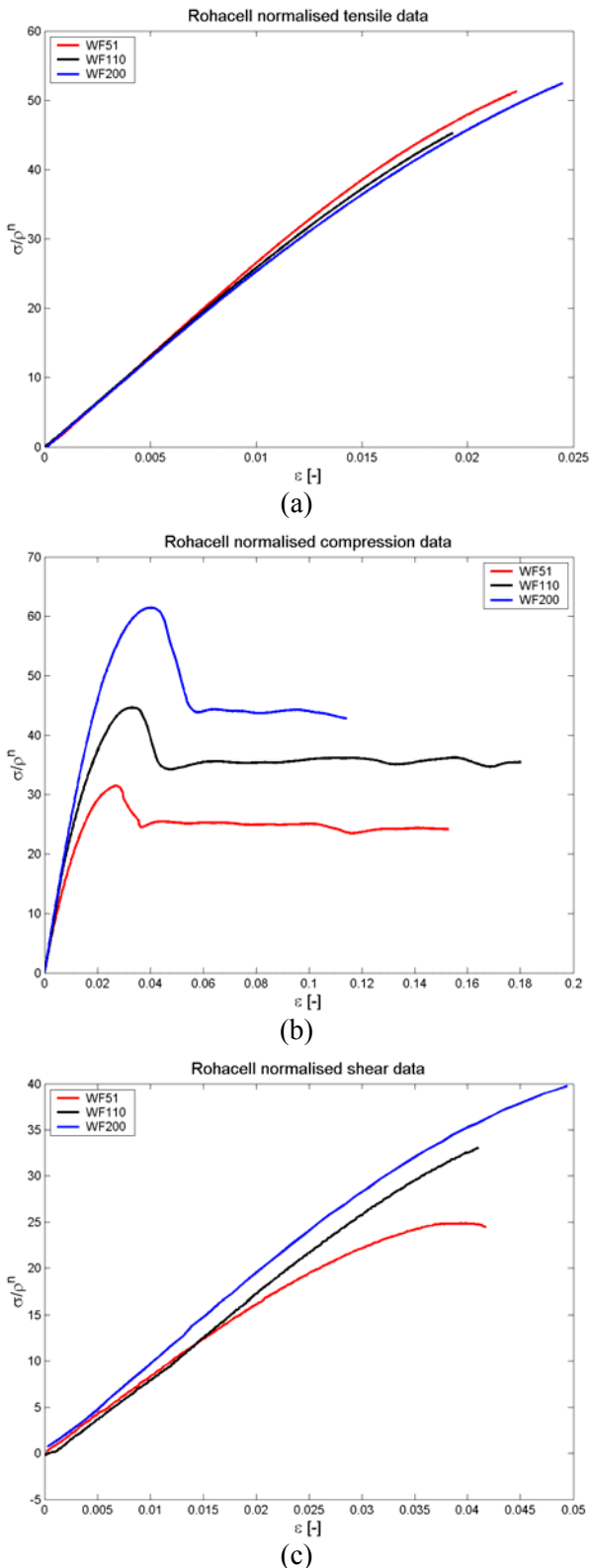

(b)

Rohacell normalised shear data

(c)

Fig. 3. Density normalized stress relations in (a) tension, (b) compression and (c) shear.

The WF51 material has a clear non-linear relation in compression for strain larger than

approximately 0.5%. For WF110 the compressive stress-strain relation starts becoming non-linear at somewhat higher strains, approximately 0.75%, whereas for the WF200 material the non-linearity starts at above 1% strain. This is also seen in Fig.3b. This non-linear part prior to the peak stress is thus most probably due to cell wall and cell edge buckling, at least for the lower densities. The higher densities have a less pronounced non-linear part which is probably due to plastic hinge formation.

3 Crack Propagation Testing

In [11] crack propagation tests of Rohacell WF51 were performed using a compact tension (CT) specimen, as illustrated in Fig. 4. The dimensions were scaled up considerably compared to a standard metallic specimen using a characteristic length $W = 225$ mm. The same specimen type was again used to extract crack propagation data for the other qualities studied herein. The test is thus performed to obtain crack propagation data in the plane of the material block.

Fig. 4. Photograph of the CT specimen.

The specimens were tested using a sinusoidal load in load control at 2 Hz at a load ratio $R = 0.1$. The crack length was monitored using a travelling microscope and measured on one surface only. Tests were done by injecting paint into the crack front, then propagating the crack some distance (several millimetres) and cracking the specimen open. It was found that the crack remains straight through the thickness of the specimen and thus one-sided measurements is sufficient. Several crack length readings were done on each specimen and the load was shed (decreasing the load) in order to vary the

stress intensity range, but keeping the stress ratio constant.

The crack propagation measurements were fitted using Paris' law

$$\frac{da}{dN} = C\Delta K_I^m \tag{2}$$

where da/dN is the crack propagation rate (in mm/cycle), ΔK_I is the stress intensity range, m is the slope of the relation in a log-log scale and C is a constant. For details on the data reduction, see [11]. The slope was found by using a least square fit to the experimental results. The slope m was found be in order of $m = 13$-14. The density normalized Paris' law relations are shown in Fig. 5, and as seen, they collapse on single generic curve.
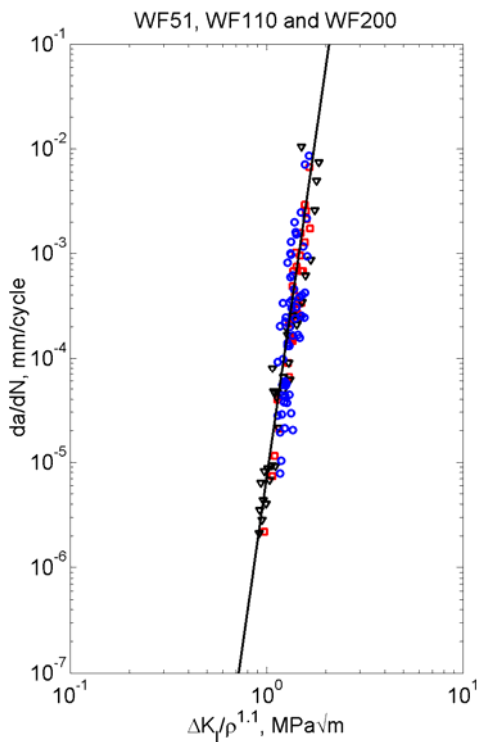

Fig. 5. Normalised da/dN vs. ΔK curves for Rohacell WF51, WF110 and WF200.

There are are two important conclusions from these test results; the crack growth rate is very high with a Paris' law exponent. Actually, very high Paris law exponents were reported on Aluminium foams [10], as high as up to $m = 25$, although the base material of the foam was aluminium which in its bulk form has a Paris law exponent in the order of 2-

4. The second is that the crack propagation can be density normalised in the same manner as static tensile data, and a generic Paris' law curve can be obtained for all densities within this class of materials.

Tension-tension Fatigue Testing

The fatigue test procedure used an axi-symmetric dog bone specimen, described in ASTM D1623-78 "Tensile and tensile adhesion properties of rigid cellular plastics" [17]. The specimens were cut from foam core blocks, bonded between two aluminium cylinders and a waist was milled to the correct shape and size in a lathe. Thus, this testing is done in the thickness direction of the foam block. The test rig with a specimen is shown in Fig. 6.
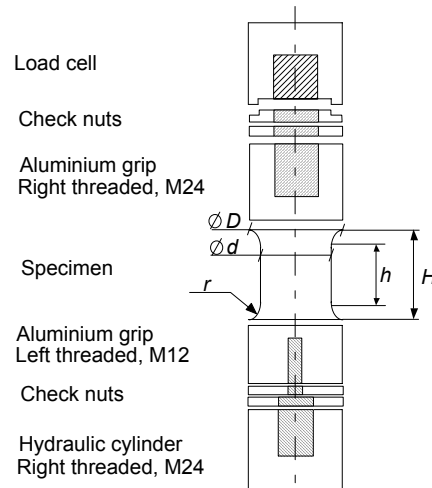

Fig. 6. Schematic drawing of the test set-up tensile fatigue specimen. Dimension used $D = 50$ mm, $d = 30$ mm, $H = 50$ mm, and $h = 32$ mm.

The fatigue tests were performed under a load controlled sinusoidal cycle using a servo hydraulic testing machine. The load ratio used was in all cases $R = \sigma_{min}/\sigma_{max} = 0.1$ and a testing frequency of 5 Hz. The fatigue life of the specimens is characterised as the number of cycles to ultimate failure.

There were no visual signs of damage in the specimens prior to failure, which occurred abruptly. Monitoring the stiffness of the specimens throughout the testing exhibited no measurable changes in stiffness up until the final load cycles prior to complete rupture [14].

Compression-compression fatigue testing

The compression-compression fatigue tests were performed using a similar set-up to the tensile fatigue testing. Cylindrical core samples (same type as in the tensile testing) were bonded to aluminium blocks and tested in fatigue at the load ratio $R = 10$ (the same as in tension but with negative loads) and with a testing frequency of 5 Hz. A photograph of the test specimen is shown Fig. 7.

Fig. 7. Photograph of compression-compression fatigue test specimen showing typical crush band fracture in compression fatigue.

A clip-gauge was mounted to the specimen to measure the displacement in each load cycle. The test was interrupted when a permanent strain of 2% was reached (1 mm permanent deformation). At such permanent strain it was found that a crush band had formed in the specimen of a thickness of at least one layer of cells. Every specimen was inspected visually to ensure that a crush band had formed once the test was interrupted. This could also be seen when plotting the maximum or minimum displacement of the clip-gauge during the test. At the formation of a crush band there was a sudden drop in displacement as shown in Fig. 8. This figure is intentionally plotted with linear axes, rather than logarithmic, so that the displacement changes appear more clearly. Actually, there are two displacements drops, first one occurring at approximately $3 \cdot 10^5$ load cycles. The drop is approximately 0.4 mm, which corresponds quite well to the average cell size of the material. The displacement drop thus indicates that one layer of cells in the specimens is being crushed and compacted. There is clear indications of a second displacement drop some 20000 cycles later, which most probably indicates that an adjacent layer of cell is crushing.
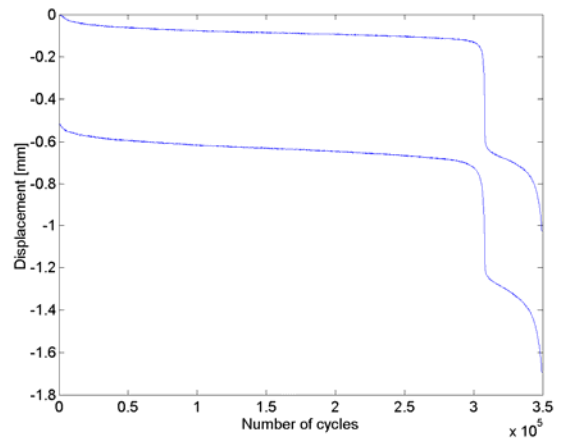

Fig. 8. displacement versus number of cycles in a compression-compression test.

In Fig. 8 one can also notice some creep deformations in the specimen. There was more creep in the compression fatigue testing for higher loads and also more pronounced creep for the lowest density (WF51) than for the higher ones.

Shear fatigue testing

A four point bending rig which enables fatigue loading with both positive and negative loads was used in this investigation, as depicted schematically in Fig. 9a. This design allows the supports to rotate around the neutral axis of the beam in order to minimise the stress concentrations near the load introductions. Furthermore the supports are movable in the beam length direction to enable varying settings of L_1 and L_2. The supports are also covered with rubber pads in order to smooth out the load transfer. The outer load arms are allowed to move horizontally thus preventing any membrane forces to occur.

The tests were performed with sandwich beam specimens, all with glass-fibre composite face sheets manufactured from non-crimp fabrics and vinylester resin using a vacuum infusion process. All specimens were 500 mm long, a width equal to the thickness, and tested using the set-up, $L_1 = 80$ mm and $L_2 = 440$ mm. For the WF51 configuration a 50 mm thick core was used with approximately 4 mm thick faces, the WF110 configuration had a 25 mm core with 2.4 mm thick faces and the WF200 configuration had a 32 mm thick core with 3 mm thick face. The testing was performed at $R = 0.1$ at a testing frequency of 2 Hz.

(a)
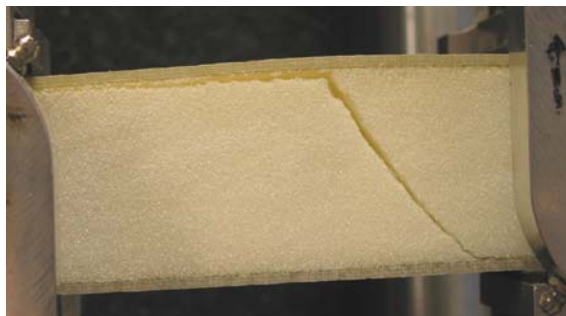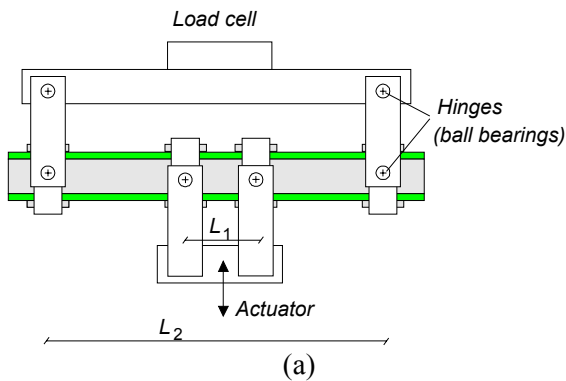
(b)

(c)

(d)

Fig. 9. (a) Four-point bending rig and fracture of (b) WF51, (c) WF110 and (d) WF200 specimens after shear fatigue

The WF200 specimens all failed by the formation of a 45-degree crack in the core, see Fig. 9d. The WF51 also had a distinct failure mode indicating that failure initiated and propagated along the face/core interface, as seen in Fig. 9b. This is

seen from the fact that the final core crack running through the thickness of the specimen has a kinking angle from the interface clearly larger than 45 degrees, rather in the order of 70 degrees. This is evidence that there has been an interfacial macro-crack present just prior to final failure, and when loaded in pure shear this is equivalent of a crack subjected to mode II loading. Such a crack should kink into the core with an angle of approximately 70 degrees. The WF110 exhibited a less consistent and less obvious failure mode, some with interface failures and some with 45-degree shear cracks, see Fig. 9c.

Results of fatigue testing

The results of the fatigue testing are shown in Figs.10a-c as standard double logarithmic stress-life relations. They are cut off at the yield strengths of the material as taken from the static testing. However, the choice of yield points was taken so that the cut-off stress provided a consistency with the obtained fatigue data. Why this cut-off stresses have been chosen as done herein requires a further investigation and is left for future work.

From the results given in Fig. 10 we can conclude several things: The stress-life data can be plotted using a Basquin's law type relation that reads

$$\Delta\sigma = B(N)^{-\beta} \qquad (3)$$

This type of relation seems to fit all the experimental results fairly well, despite obvious experimental scatter. If done so, the life expectancy at yield strength is approximately 10^2 cycles, or at least in that order of magnitude, i.e. the linear stress-life curve crosses the horizontal cut-off corresponding to the yield strength at approximately 100 cycles to failure.
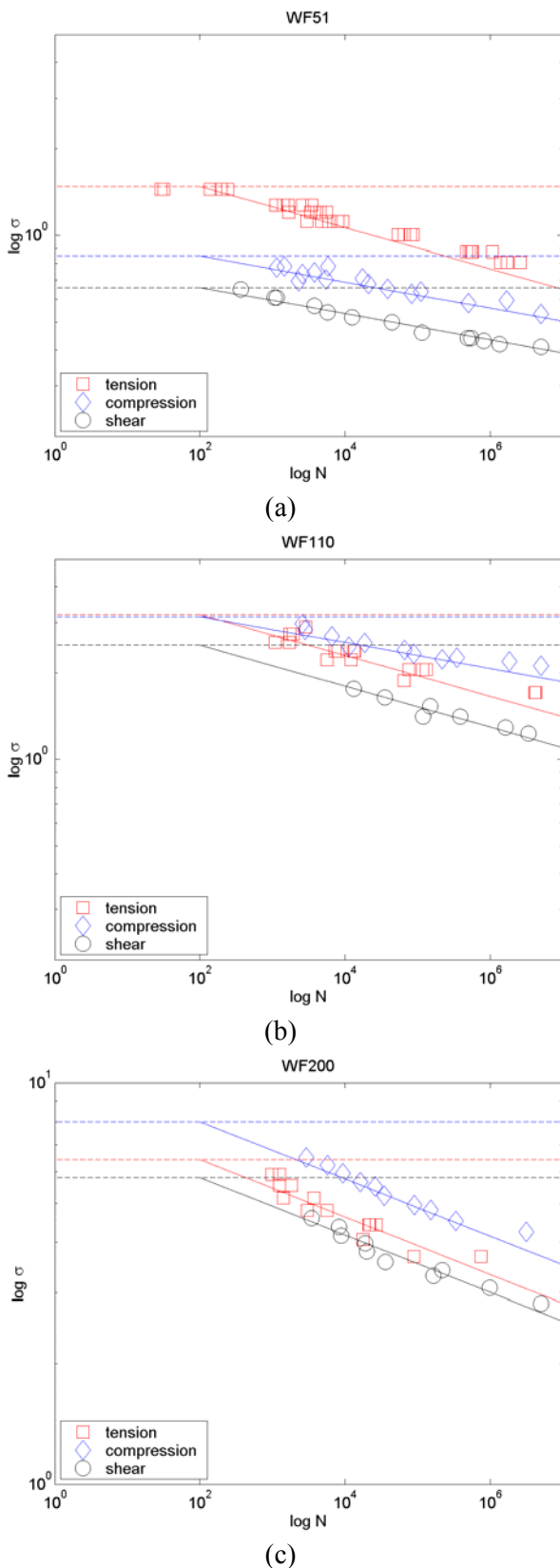
Fig. 10. Fatigue stress-life diagrams for (a) WF51, (b) WF110 and (c) WF200.

One can observe that for the lower density foam (WF51) the S-N curve in shear is close to that in compression. This relates well to the static results for which the compression strength is lower than the tensile strength due to the buckling dominated failure mechanism in compression. Since shear is a combination of tension and compression it is likely that the shear fatigue results should compare well with the fatigue curve in compression.

For the higher densities, however, the situation is different. For WF110, the S-N curve in compression is higher than both the shear and the tensile S-N curves and shear still below the shear fatigue curve. This follows the static results. For WF200, the compressive strength is higher than the tensile strength, and logically we see that the S-N (stress-life) curve in compression is above that in tension, with the shear S-N curve underneath.

The slope of all S-N curves is another interesting feature. In [14] it was concluded that the slope of the Paris' law curve for the material could be translated to the slope of the S-N curve so that the Paris' law slope m is translated to the slope of the S-N curve through $\beta = -1/m$. Actually, by taking the tensile S-N curves in Fig. 10 and making a best fit to the test results, it can be seen that m is around 14-15 ($\beta = -1/14$ -- $-1/15$). In Fig. 10 $m = 14$ has been used. By having a look at the individual densities one can see the following. For WF51 the tensile S-N curve has a slope $m \approx 14$ whereas the compressive and shear curves have a lower slope (higher m) that is closer to 20 (23 in compression and 20 in shear from a best fit). There is some logic to this, although the behaviour is not clear at this moment. The most probable reason is that the failure mechanism is different in tension to that in compression and shear, thus resulting in different slopes. Shear and compression should exhibit the same failure mechanism and seems to have approximately the same slope. In tensile loading the cell edges and walls will stretch and bend, whereas in compression and shear the dominating deformation mechanism is most likely buckling.

For WF110 the results are a little more difficult to interpret. The tensile S-N curve has the same slope as the other tensile data. In shear, the slope is the same as in tension, but at a lower stress level. The compression fatigue data has the highest stress level and a lower slope with $m \approx 24$ from curve fitting. This value is almost the same as for WF51 in compression (and shear). It seems likely that the failure mechanism in shear is the same as in tension, being closer in stress and having the same slope. The

failure mechanism in compression seems to the same as in compression for WF51.

For WF200 the picture is clearer. All S-N curves have the same slope with $m \approx 14$. The tension and shear curves almost overlap. The compression fatigue data has the same slope but at a higher stress value. This indicates that this higher density material exhibits the same principal failure mechanism in all load cases and that buckling of cell edges and cell walls has little influence on the behaviour.

Discussion

First, let's have a look at the static properties of these foams. In tension, the static stress-strain relations can be density normalized to collapse into one single relation (Fig.3a). However, the compressive stress-strain curves do not seem to do this at all (Fig.3b). The reason for this is the different failure mechanisms in tension and compression. In tension, the cell edges and walls in the foam undergo plastic strains and rupture. This mechanism is cell size and cell wall/edge thickness independent. The crack propagation data can also be density normalised using the same normalisation exponent (1.1), as shown in Fig. 5. The tensile S-N curves for all densities can be treated the same way and will then collapse into one single generic S-N curve [14], which is shown in Fig.11a. The same approach was used for another foam, Divinycell H-grade, in [14].

In compression, on the other hand, cell wall buckling is most probably the dominating mechanism of deformation, at least for the lower density foams. For higher density foams, the cell walls are both smaller and thicker, suppressing buckling. This explains why the compression strength is much lower than the tensile strength for the lower density foam. The normalised fatigue data in compression and shear are shown in Fig. 11b and 10c. They do not collapse into one single generic curve. In compression there is no correlation at all with the two lower densities having a different slope than WF200. However, the WF110 and WF200 are pretty close in terms of normalised stress (Fig.11b) but with different slopes. In shear we see that the WF110 and WF200 normalised fatigue life curves have the same slope, but at slightly different magnitudes. The discrepancy could either be that the there is some influence from cell wall buckling or simply that the density scaling is different in shear.
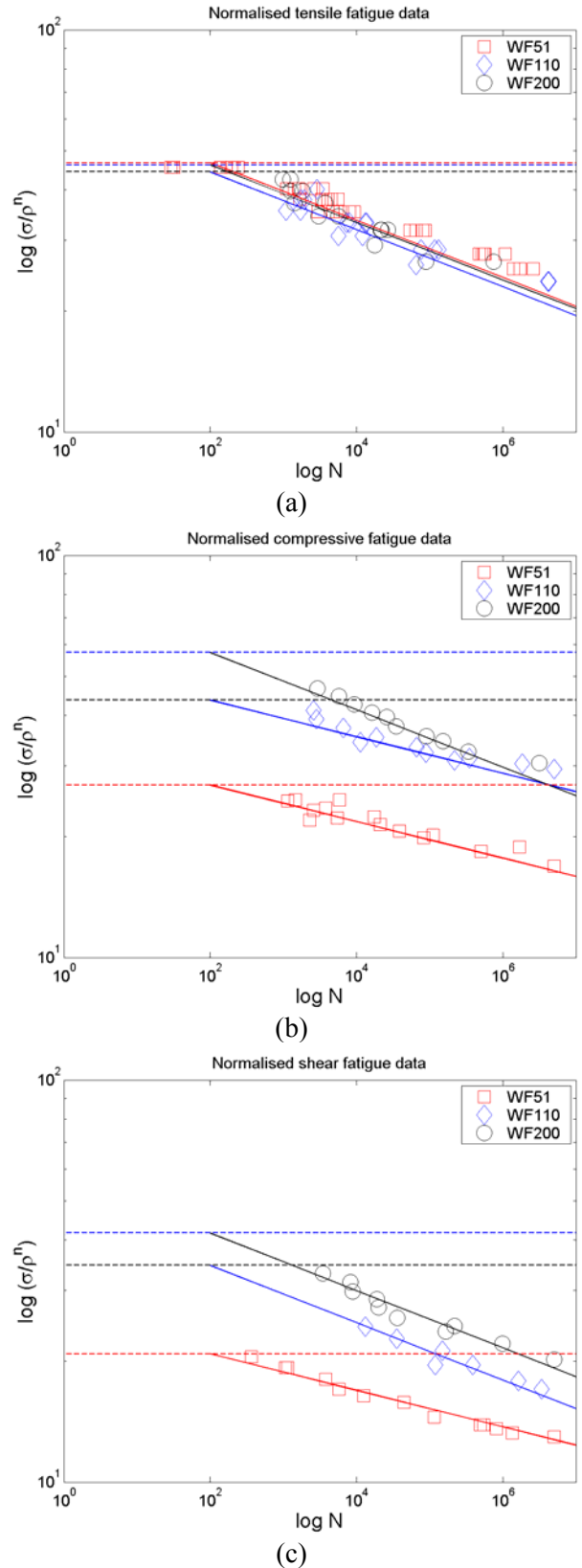

(a)

(b)

(c)

Fig. 11. Density scaled S-N curves for WF51, WF110 and WF200, (a) tension, (b) compression and (c) shear.

An open pending question that cannot be answered at this point is how the failure mechanism in shear fatigue loading actually looks and eventually leads to failure for the lower density foams. The face/core interface separates (debonding failure) after a certain number of loading cycles, but why at the interface and what is the local failure mechanism at cell size level? This is a question for future research.

Acknowledgements

References

[1] Burman M. and Zenkert D., "Fatigue of Foam Core Sandwich Beams, Part I: Undamaged Specimens", *Int. J. Fatigue*, Vol, 19, No 7, pp 551-561, 1997.

[2] Burman M. and Zenkert D., "Fatigue of Foam Core Sandwich Beams, Part II: Effect of Initial Damages", *Int. J. Fatigue*, Vol, 19, No 7, pp 563-578, 1997.

[3] Shenoi R.A., Clark S.D. and Allen H.G., "Fatigue Behaviour of Polymer Composite Sandwich Beams", *J. of Comp. Mat.*, Vol.29, No.18, pp 2423-2445, 1995.

[4] Buene L., Echtermeyer A.T. and Sund O.E, "Fatigue Properties of PVC Foam Core Materials", *Det Norske Veritas Report 91-2049*, 1991.

[5] K. and Mahfuz H., "Flexural fatigue characteristics of sandwich structures at different loading rates", *Comp. Struct.*, Vol.67, No 4, pp 403-410, 2005

[6] Kanny K., Mahfuz H., Carlsson L.A., Thomas T. and Jeelani S., "Dynamic mechanical analyses and flexural fatigue of PVC foams", *Comp. Struct.*, Vol.58, No 2, pp 175-183, 2002.

[7] Kulkarni N., Mahfuz H., Jeelani S. and Carlsson L.A., "Fatigue crack growth and life prediction of foam core sandwich composites under flexural loading", *Comp. Struct.*, Vol.59, No 4, pp 499-505, 2003.

[8] McCullough K.Y.G., Fleck N.A. and Ashby M.F., "The stress-life fatigue behaviour of aluminium alloy foams", *Fatigue and Fracture of Eng. Mat. & Struct.*, Vol.23(3), pp 199-208, 2000.

[9] Harte A.-M., Fleck N.A. and Ashby M.F., "Fatigue Failure of an Open and a Closed Cell Aluminium Alloy Foam", *Acta Mater..*, Vol 47, No 8, pp 2511-2524, 1999.

[10] Olurin O.B., McCullough K.Y.G., Fleck N.A. and Ashby M.F., "Fatigue Crack Propagation in Aluminium Alloy Foams", *Int. J. Fatigue*, Vol 23, No 5, pp 375-382, 2001.

[11] Shipsha A., Burman M. and Zenkert D., "On Mode I Fatigue Crack Growth in Foam Core Materials for Sandwich Structures", *J. of Sandwich Struct. & Mat.*, Vol 2, No 2, pp 103-116, 2000.

[12] Shipsha A., Burman M. and Zenkert D., "Interfacial Fatigue Crack Growth in Foam Core Sandwich Structures", *Fatigue and Fracture of Eng. Mat. & Struct*, Vol 22, No 2, pp 123-131, 1999.

[13] Huang J.S. and Lin J.Y., "Fatigue of Cellular Materials", *Acta Mater.*, Vol 44, No 1, pp 289-296, 1996.

[14] Zenkert D., Shipsha A. and Burman M., "Fatigue of Closed Cell Foams", *J. of Sandwich Struct. & Mat.*, Vol 8 (6), pp 517-538, 2006.

[15] *Rohacell WF*, Röhm Degussa-Hüls group, www.roehm.com

[16] Gibson L.J. and Ashby M.F., *Cellular Solids – Structure and Properties*, 2:nd edition, Cambridge University Press, Cambridge, UK, 1997.

[17] *Annual Book of the ASTM Standards,* American Society for Testing and Materials, Philadelphia, PA.